

Ultrathin SiO₂ on Si. VI. Evaluation of uncertainties in thickness measurement using XPS

M. P. Seah*

Quality of Life Division, National Physical Laboratory, Teddington, Middlesex TW11 0LW, UK

Received 26 July 2004; Revised 3 November 2004; Accepted 5 November 2004

Measurements of the thicknesses of SiO₂ on Si in the range 1.5–8 nm can be made by XPS with precisions as high as 0.025 nm at one standard deviation, but in the past this has been overshadowed by systematic uncertainties of the order of 20% of the thickness arising from the uncertainty in the relevant electron attenuation length. This is shown no longer to be the case. An analysis is presented, of the contributions to the measurement precision arising from the counting statistics, peak fitting and setting of the emission angle for the detected electrons. With traditional commercial equipment, the angle-setting accuracy of 0.5° can be the limiting factor. For comparison between laboratories, further terms degrade the comparability: a typical 1% from the consistency of any samples used for the comparison; a more significant term from the angular acceptance of those spectrometers that accept more than ±10° of the emission angles; contributions from the variability of the procedures for analysing the peak intensities for the quantification; and variations in the algorithms used. For absolute quantification in the above thickness range, a recent calibration of the attenuation length enables the uncertainty to be kept to ~2% at 95% confidence but the above variability in procedures in general analytical laboratories leads to this value degrading often to as poor as 0.4 nm, again at 95% confidence. © Crown Copyright 2005. Reproduced with the permission of Her Majesty's Stationary Office. Published by John Wiley & Sons, Ltd.

KEYWORDS: ARXPS; gate oxides; silicon dioxide; SiO₂; thickness measurement; uncertainties; XPS

INTRODUCTION

The surface analysis methods^{1,2} are powerful methods for research in fields ranging from microelectronics and defence to biotechnology and the life sciences. In the hands of skilled researchers and analysts, the volume of published cutting edge research, industrial product development and quality control continues to grow. Vital for the latter are the excellent precision and repeatability of the methods, and as equipment and procedures develop these will improve further. An essential mechanism to deliver the procedures to enhance consistency is the activity of ISO technical committee 201 on Surface Chemical Analysis. Here procedures have been developed to evaluate the repeatability for Auger electron spectroscopy (AES)³ and x-ray photoelectron spectroscopy (XPS),⁴ and typically better than 1% should be achievable in most laboratories. Procedures for static secondary ion mass spectrometry (SSIMS) are under development.^{5,6}

For quantitative correlations of measurements between methods or between one method and theory, we need both linearity and accuracy. Methods have been derived to evaluate the linearity of electron spectrometers^{7,8} but the issue of accuracy is more difficult to address by a general, widespread study. Surface analysis instruments are

all physically based beam methods that have no issues of sample extraction or other steps in the analytical procedure and so, provided that we understand the physics of the signal production, all can be traceable and accurate methods. In chemical analysis, generally, accuracy is often delivered by calibration using certified reference materials (CRMs). However, if we understand the physics of the analytical method and can calculate all parameters, the methods become accurate without the use of CRMs. If individual parameters cannot be calculated accurately, but can be measured by other methods, again CRMs may be avoided. If certain aspects are very sensitive to the instrument settings, it may be that CRMs cannot be avoided in calibrating the instrumental response for a given analysis. In general, we try to avoid the use of CRMs, even if slightly poorer accuracy is achieved, because the costs of CRMs are high in this area and the calibration is specific to the system of the CRM. For evaluation of depth profiles of dopants in semiconductors by SIMS, reference materials, certified or otherwise, cannot be replaced yet by direct calculational routes.

To evaluate the issue of accuracy in XPS, we have focused on measurement of the amount of substance of silicon oxides on silicon, expressed as the thickness of SiO₂ in nanometres. A broad intercomparison has been completed involving 45 sets of measurements in different laboratories involving the following 10 methods: medium-energy ion scattering spectrometry (MEIS), neutron reaction analysis (NRA), Rutherford backscattering spectrometry

*Correspondence to: M. P. Seah, Quality of Life Division, National Physical Laboratory, Teddington, Middlesex TW11 0LW, UK.
E-mail: martin.seah@npl.co.uk
Contract/grant sponsor: UK Department of Trade and Industry.

(RBS), elastic backscattering spectrometry (EBS), XPS, SIMS, ellipsometry, grazing incidence x-ray reflectometry (GIXRR), neutron reflectometry and transmission electron microscopy (TEM).^{9,10} The intercomparison was based on carefully grown thermal oxides with defined and low levels of contamination,¹¹ with the oxide thicknesses controlled to 1% for the different participants.^{12,13} A prior study by Cole *et al.*¹⁴ indicated that at a thickness of 4 nm we may have expected a scatter of 2 nm, but the results in our more recent study turned out to be significantly better. Respondee results, $d_{\text{respondee}}$, were compared against NPL reference data, d_{RT} , based on XPS and ellipsometry, using a straight-line relation of the form

$$d_{\text{respondee}} = m_{\text{respondee}} d_{\text{RT}} + c_{\text{respondee}} \quad (1)$$

where $m_{\text{respondee}}$ or $c_{\text{respondee}}$ were the scaling and offset constants to be evaluated for each of the 45 data sets. The study showed that the average root-mean-square (rms) scatter about this correlation was 0.15 nm and that half were better than 0.1 nm and a few better than 0.05 nm. Some of the higher scatters arose simply from low counting statistics, particularly in RBS. The main methods used were all linear in Eqn. (1) except for SIMS in the thickness regime below 2 nm.

The XPS results used a wide variety of geometries and it was known that this would lead to very scattered results.¹² Laboratories responding early were thus asked to supply a second set of data using a defined reference geometry.¹² Eight sets of XPS data for the reference geometry were received, as shown in Table 1, in addition to one extra from NPL. These exhibited a very much improved scatter, despite the variety of methods for calculating the thickness of the oxide. The procedure used at NPL is described in detail elsewhere.^{10,15} Briefly, to reduce the effects of forward focusing, measurements are recorded for the reference geometry at an emission direction defined to be at the centre of the stereographic triangle for both the (100) and (111) surfaces. This was at 34° to the surface normal in an azimuth at 22.5° to one of the edges of the

square (100) samples or at 25.5° from the surface normal in an azimuth of one of the edges of the triangular (111) samples. The cleaved edges are (111) planes defining the [110] directions. For a spectrum such as that shown in Fig. 1, prior to peak fitting, the x-ray satellites were removed together with the 2p_{3/2,1/2} spin-orbit splitting determined as 50% of the intensity at 0.60 eV higher binding energy.¹⁶ The remaining structure was evaluated as five peak intensities— I_{Si} , $I_{\text{Si}_2\text{O}}$ at 0.95 eV higher binding energy (BE), I_{SiO} at 1.75 eV higher BE, $I_{\text{Si}_2\text{O}_3}$ at 2.48 eV higher BE and I_{SiO_2} at 3.96–4.36 eV higher BE—as defined by Hollinger and Himpfel¹⁶ and by Keister *et al.*¹⁷ These peaks were fitted with peak energies fixed, as indicated, in relation to the Si peak. Note that the SiO₂ peak was allowed to move in a small range to higher BE as the film thickness increased. The peak fitting was simultaneous with removal of a Shirley background,¹⁸ with a 15-point smooth inwards from the end points at 8.2 eV higher and 2.7 eV lower BE than the Si 2p peak. All peak full widths at half-maxima (FWHMs) were constrained to be in the range 0.7–1.5 eV.

The thickness d of a uniform layer of oxide may be calculated using the well-known relation for photoelectrons from the metal and oxide states of a single peak

$$d = L \cos \theta \ln(1 + R_{\text{expt}}/R_0) \quad (2)$$

where d is the oxide thickness, L is the attenuation length of the substrate and oxide photoelectrons in the oxide, R_{expt} is the ratio of the measured intensities of the photoelectrons from the oxide and the elemental states from the sample and R_0 is the ratio of these intensities from bulk materials. From Fig. 1 we see that there are intermediate oxides and a carbonaceous overlayer. The carbonaceous layer is established to be on the outside of the material and most of it may be removed by solvent washing.⁹ The final part of this contamination can be removed by using ultraviolet light with ozone, but that is not done here because it may also change the oxide layer. Fortunately, the contamination has no effect on our analysis.¹² The intermediate oxides are known to exist at the interface because a certain distribution

Table 1. Parameters used in XPS analysis of the oxide thicknesses in the interlaboratory study¹⁰

| Laboratory | Instrument | X-rays ^a | γ^b | Background ^c | I_{Si}^∞ | No. of peaks | $m_{\text{respondee}}$ | $c_{\text{respondee}}$ (nm) | $r_{\text{respondee}}$ (nm) |
|-------------------|-------------------|---------------------|------------|-------------------------|------------------------|--------------|------------------------|-----------------------------|-----------------------------|
| BAM | SSX-100 | Al* | 71° | Shirley | 242 000 | 3 | 0.995 | 0.026 | 0.052 |
| NRC | Kratos Axis Ultra | Al* | 54° | SL/O | 382 000 | 2 | 0.981 | −0.171 | 0.094 |
| U. of Utsunomiya | PHI 5600 | Al* | 90° | Shirley | 37 000 | 2 | 1.030 | 0.043 | 0.084 |
| Nat. U. Singapore | VG Escalab II | Mg | 49° | SL | 183 000 | 4 | 1.036 | 0.012 | 0.136 |
| CSIR | PHI Quantum | Al* | 45° | Shirley | 49 000 | 2 | 1.000 | −0.178 | 0.115 |
| EMPA | PHI Quantum | Al* | 45° | Shirley | 19 000 | 2 | 1.018 | −0.177 | 0.084 |
| NPL | VG Escalab II | Mg | 55° | Shirley | 800 000 | 5 | 0.998 | 0.025 | 0.019 |
| Philips 1 | PHI Quantum | Al* | 45° | Shirley | 87 000 | 5 | 0.952 | 0.101 | 0.056 |
| Philips 2 | PHI Quantum | Al* | 45° | Shirley | 52 000 | 5 | 0.969 | 0.128 | 0.054 |
| Average | | | | | 206 000 | | 0.998 | −0.021 | 0.077 |
| SD | | | | | | | 0.028 | 0.121 | |

^a Al* = monochromated Al x-rays.

^b Included angle between incident x-rays and emitted electrons.

^c SL = straight-line background; O = oversmooth background.

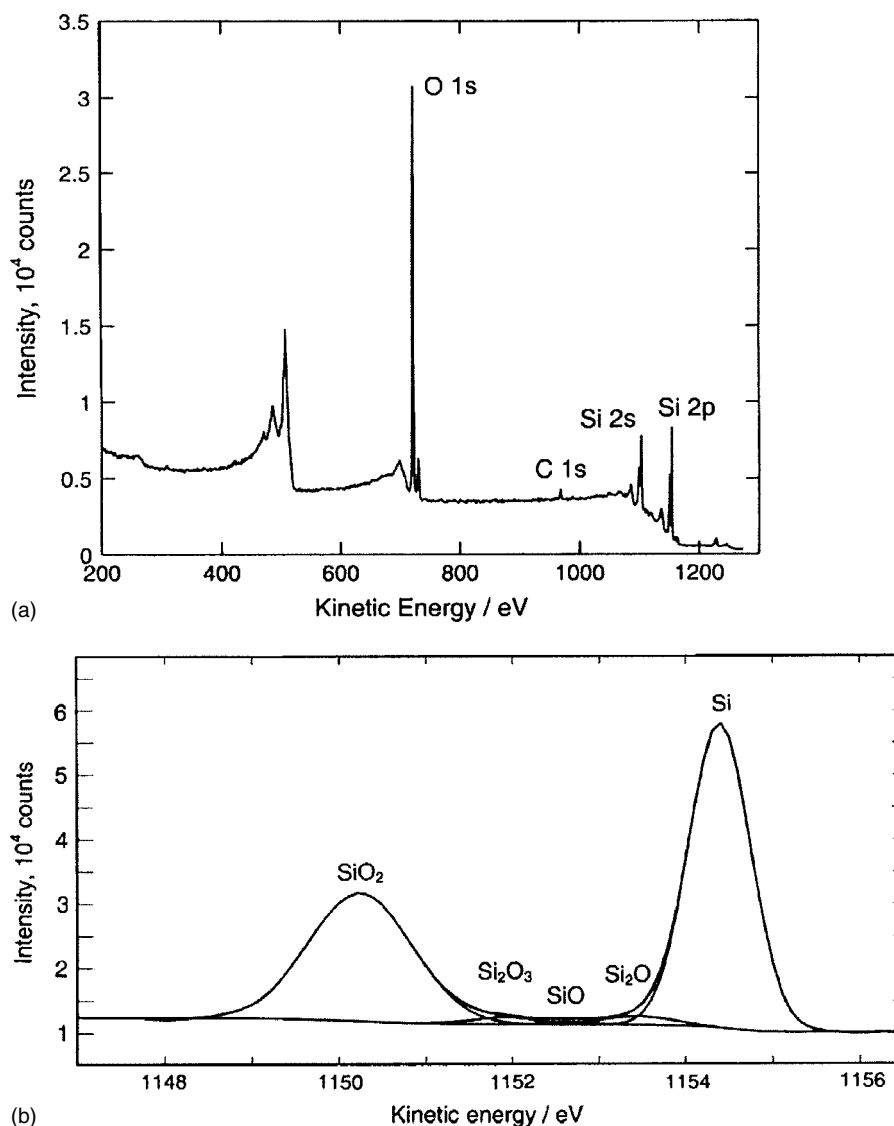


Figure 1. The XPS spectrum for a cleaned¹¹ sample with ~ 2 nm of oxide, analysed using Mg $K\alpha$ x-rays at the reference geometry:¹² (a) widescan; (b) Si 2p peaks after satellite and spin-orbit removal, showing the Shirley background and the synthesis with five peaks.

of amounts of different intermediate states is required as a result of the physical joining of a layer of SiO₂ to the Si lattice. We assume here, as shown later, that all of the intermediate oxides are in a very thin layer between the SiO₂ and the Si. With this structure comprising an overlayer of SiO₂ over the intermediate oxides, which are in turn over the Si lattice, we need to replace Eqn. (2) by the following four equations¹⁵

$$d_{\text{SiO}_2} = L_{\text{SiO}_2} \cos \theta \ln \left[1 + \left(\frac{\frac{I_{\text{SiO}_2}}{R_{\text{SiO}_2}}}{\frac{I_{\text{Si}_2\text{O}_3}}{R_{\text{Si}_2\text{O}_3}} + \frac{I_{\text{SiO}}}{R_{\text{SiO}}} + \frac{I_{\text{Si}_2\text{O}}}{R_{\text{Si}_2\text{O}}} + I_{\text{Si}}} \right) \right] \quad (3)$$

$$d_{\text{Si}_2\text{O}_3} = L_{\text{Si}_2\text{O}_3} \cos \theta \ln \left[1 + \left(\frac{I_{\text{Si}_2\text{O}_3}}{R_{\text{Si}_2\text{O}_3} I_{\text{Si}}} \right) \right] \quad (4)$$

$$d_{\text{SiO}} = L_{\text{SiO}} \cos \theta \ln \left[1 + \left(\frac{I_{\text{SiO}}}{R_{\text{SiO}} I_{\text{Si}}} \right) \right] \quad (5)$$

$$d_{\text{Si}_2\text{O}} = L_{\text{Si}_2\text{O}} \cos \theta \ln \left[1 + \left(\frac{I_{\text{Si}_2\text{O}}}{R_{\text{Si}_2\text{O}} I_{\text{Si}}} \right) \right] \quad (6)$$

with

$$d_{\text{oxide}}(5P) = d_{\text{SiO}_2} + 0.75 d_{\text{Si}_2\text{O}_3} + 0.5 d_{\text{SiO}} + 0.25 d_{\text{Si}_2\text{O}} \quad (7)$$

Equations (4), (5) and (6) simply reflect the application of Eqn. (2) to the intermediate oxides in the very thin interfacial layer. Anything above this layer attenuates the intermediate oxide and substrate peaks equally and so may be ignored. Equation (3) is a variant of Eqn. (2) where the substrate intensity now needs to include the contributions from the intermediate oxides that are, effectively, part of the substrate. In evaluating these equations earlier,¹⁰ it was shown that the difference between d_{oxide} and d_{SiO_2} (measured for 10 thermal oxides from different sources and for different orientation substrates) is 0.128 ± 0.008 nm. This is close to the value of 0.124 nm expected for an abrupt interface¹⁰ and confirms the model proposed.

In Eqn. (7), the 5P in parentheses denotes calculation by, in this case, the five-peak method rather than the two-peak method of Eqn. (2). Equation (7) effectively says that a layer

of, say, $d_{\text{Si}_2\text{O}_3}$ is equivalent to a layer of thickness $0.75 d_{\text{Si}_2\text{O}_3}$ of SiO_2 and a layer of thickness $0.25 d_{\text{Si}_2\text{O}_3}$ of Si. This mimics what an analytical method concerned with the amount of oxygen reacted with Si would do.

There are no calculations or data for values of R and L for the intermediate oxides, and so here we merely interpolate linearly from SiO_2 to Si. In this way

$$R_{\text{Si}_2\text{O}_x} = 1 + 0.25X(R_0 - 1) \quad (8)$$

and for Mg x-rays, if R_0 is taken as 0.9329^{9,10}

$$R_{\text{Si}_2\text{O}_x} = 1 - 0.016775X \quad (9)$$

For Mg $K\alpha$ x-rays, $L_{\text{Si}} = 2.415$ nm and $L_{\text{SiO}_2} = 2.964$ nm, so that

$$L_{\text{Si}_2\text{O}_x} = 2.415 + 0.13725X \quad (10)$$

If a linear interpolation is not used, the calculated thicknesses increase by 0.007 nm.¹⁰

Not all the responding laboratories used this procedure:¹⁰ NRC used a combination of straight-line and oversmoothed backgrounds that were available in their Kratos software; other laboratories used fewer peaks and ignored the interface oxides (as shown in Table 1), in which case Eqn. (2) was used. Calculations shown elsewhere¹⁵ can be used to show that, for two peaks with x-ray satellite subtraction and spin-orbit contributions removed in the range 1.5–8 nm, m is increased by 0.014 with c reduced by 0.018 nm, whereas with three peaks and no spin-orbit subtraction m is reduced by 0.008 and c is increased by 0.015 nm.

One important item shown in Table 1 is the signal level, given as the peak area in total counts. We have shown elsewhere¹² that for any fixed operating condition of the spectrometer the total equivalent signal from any of the oxides, I_{Si}^∞ , is given approximately by

$$I_{\text{Si}}^\infty = \frac{I_{\text{SiO}_2}}{R_0} + I_{\text{Si}} \quad (11)$$

Thus I_{Si}^∞ is a useful parameter to characterize the signal level in the experiment and from which statistical uncertainty measurements may be evaluated. The value of I_{Si}^∞ is given in Table 1.

The statistical terms lead to random contributions to the overall uncertainty in XPS, U . The different numbers of peaks used in the analysis procedures shown in Table 1 lead to the biases described above. Below, we shall consider these and other contributions to U . In this work we shall sum all uncertainties in quadrature unless specified otherwise. Many uncertainties are of the order of 1% of the thickness but others do not scale with that thickness. The uncertainty, U , in a given laboratory has contributions from the counting statistics, U_n , and the standard deviation, σ_θ , for setting the angle of emission, θ . These two contributions define the measurement repeatability that may be obtained in that laboratory. Further contributions to the accuracy then arise from: any bias in the setting of θ ; the angular averaging of the entrance solid angle of the spectrometer input lens, U_A ; differences between peak-fitting algorithms, U_F ; the use

of different numbers of peaks, U_P ; any bias in the value of the attenuation length used, U_L ; and any effect of the photoelectron anisotropy, U_β . These bias effects are all type B uncertainties¹⁹ rather than the statistical, precision, type A uncertainties leading to the scatters measured in repeatability tests. The type B uncertainties are difficult to evaluate in a single laboratory but may be assessed from theory and from interlaboratory studies.

In addition to the above uncertainties are the non-linearity of the detector^{7,8,20,21} and the non-linearity of Eqns (3)–(6). The Si 2p peak used here is relatively weak. Non-linearities arising from detector effects are calculated to be insignificant for the results discussed here.^{7,8,20} The non-linearities of Eqns (3)–(6) are calculated to be less than ± 0.025 nm in the thickness range studied here¹⁵ and, because we shall be dealing with terms significantly greater than 0.025 nm, will be ignored.

It is useful, first, to evaluate the uncertainties that one laboratory will encounter arising from the repeatability of instrument settings and of the counting statistics.

UNCERTAINTIES ARISING FROM THE COUNTING STATISTICS AND THE INSTRUMENT SETTINGS—THE REPEATABILITY

Counting statistics

Here we adopt the model for the peak structure described elsewhere¹⁵ and shown in Fig. 2, comprising two Gaussian

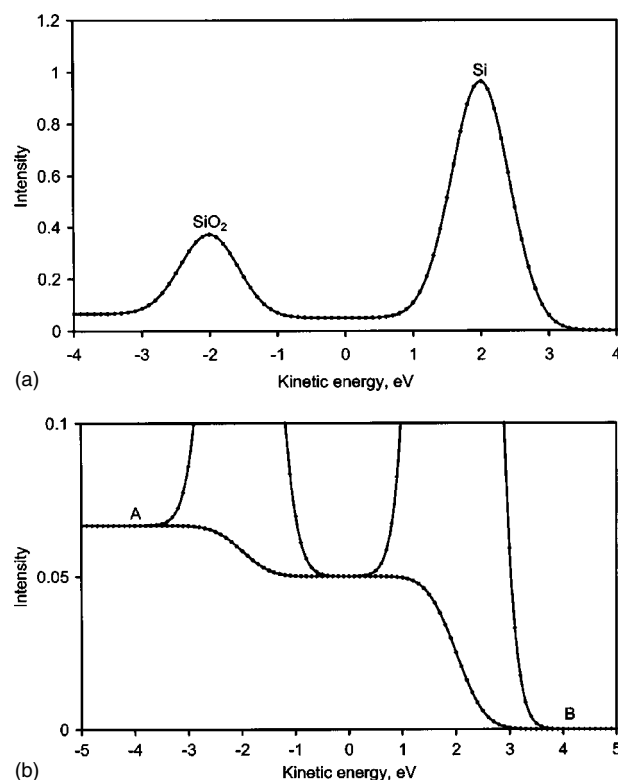


Figure 2. Synthetic spectrum of two Gaussian peaks with full widths at half maxima of 1 eV separated by 4 eV on a Shirley background with an intensity in counts of 0.05 times the peak areas to higher energy in counts · eV: (a) the spectrum; (b) detail of the background.

peaks of areas A_{SiO_2} and A_{Si} , separated by 4 eV, superimposed on a Shirley background. The spectrum has N_i counts in channel i and p channels per electron-volt. We assume that the counts exhibit a Poissonian distribution, although experimental measurements generally show that the effects of extraneous sources lead to noise generally greater than deduced from $N_i^{0.5}$ for $N_i < 100$ or $N_i > 100\,000$. At this stage we ignore the interface oxides.

Here, in fitting the two Gaussian peaks superimposed on the Shirley background, the background is assumed to be fitted first at points A and B and then subsequently the two areas are measured. This represents the case for some software systems. Others fit the Shirley background at the same time as the peaks and this can lead to significantly better results in certain well-defined situations. The measured peak shapes are, of course, not true Gaussians and some software systems may use Gauss–Lorentz sum functions whereas others use product functions.²² Both fit very well but more critical is the way the background is fitted, which, as we shall see, significantly affects both the measurement repeatability and precision.

For the above model, the uncertainties in A_{SiO_2} and A_{Si} are given by U_{SiO_2} and U_{Si} , where

$$U_{\text{SiO}_2}^2 = \{[A_{\text{SiO}_2} + 4p(0.75 N_A + 0.25 N_B)]^{0.5}\}^2 + \left[1.064p \left(\frac{0.75 N_A + 0.25 N_B}{m}\right)^{0.5}\right]^2 \quad (12)$$

and

$$U_{\text{Si}}^2 = \{[A_{\text{Si}} + 4p(0.25 N_A + 0.75 N_B)]^{0.5}\}^2 + \left[1.064p \left(\frac{0.25 N_A + 0.75 N_B}{m}\right)^{0.5}\right]^2 \quad (13)$$

The first term in these equations arises from the uncertainty in the total counts in the peak and background, whereas the second term is the uncertainty arising from errors in the background when defining points A and B. Depending on the fitting algorithm, the latter uncertainty can be a fractional error in A_{SiO_2} and A_{Si} , approximately in proportion to the peak height or the peak area. This latter fraction then leads to a $1.064p$ or a p contribution; for safety, the $1.064p$ term is used here.

Equations (12) and (13) are based on the uncertainty for Poissonian counts N being $N^{0.5}$, so that the contribution to U^2 is $\{[N]^{0.5}\}^2$ or N . However, the background to be subtracted in each channel uses data that are correlated and therefore add linearly to give the form $\{b[B]^{0.5}\}^2$ or b^2B . This means that it is critical to reduce the noise contribution of the background, and hence we average over the m points at each end.

In Eqns (12) and (13) the areas are not given in units of counts · eV but simply as the sum of the counts in the relevant channels. To improve the signal quality, the Shirley background has been smoothed over m points at A and B (taken outwards from A and B rather than inwards as with commercial software). To evaluate Eqns (12) and (13) we note that, approximately

$$N_A = 0.1(A_{\text{SiO}_2} + A_{\text{Si}})/p \quad (14)$$

$$N_B = 0.05(A_{\text{SiO}_2} + A_{\text{Si}})/p \quad (15)$$

and

$$I_{\text{Si}}^\infty = \frac{A_{\text{SiO}_2}}{R_0} + A_{\text{Si}} \quad (16)$$

Equations (14) and (15) are good approximations for unmonochromated spectra but for monochromators N_B is approximately halved. Using the simple, two-peak equation

$$d = L \cos \theta \ln \left(1 + \frac{A_{\text{SiO}_2}}{R_0 A_{\text{Si}}}\right) \quad (17)$$

with $L = 2.964$ and 3.448 nm for Mg and Al x-rays, respectively, $R_0 = 0.9329$ and $\theta = 34^\circ$,^{10,12} we may calculate the uncertainty, U_n , in d for various values of d in the range 0–8 nm. We assume here that U_{SiO_2} and U_{Si} are uncorrelated, although changes in the background do weakly affect both peaks at the same time and in the same way. This effect leads to a very small reduction in U_n compared with the present

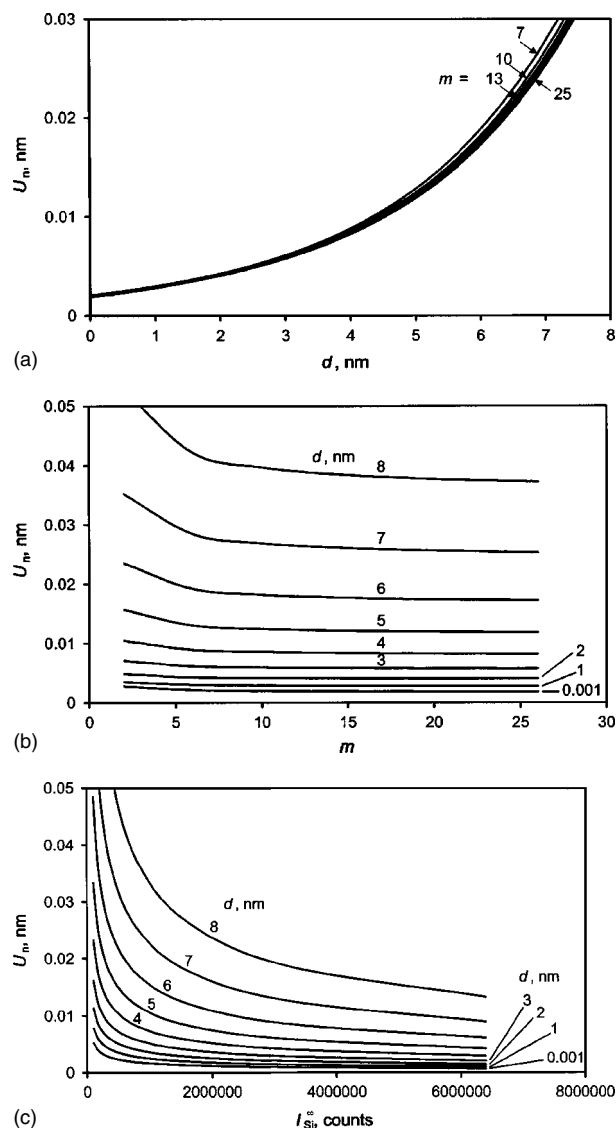


Figure 3. Standard uncertainty, U_n , arising from counting statistics for layer thicknesses in the range 0.001–8 nm: (a) as a function of d for various values of m and $I_{\text{Si}}^\infty = 800\,000$; (b) as a function of m for $I_{\text{Si}}^\infty = 800\,000$; (c) as a function of I_{Si}^∞ for $m = 25$.

evaluation. The effect of the counting statistics is shown in Fig. 3(a) as a function of thickness for Mg x-rays for a p value of 10 channels per electron-volt, for $I_{\text{Si}}^{\infty} = 800\,000$ and for various values of m . The calculations stop at 8 nm because the Si peak is then small and the uncertainties rise rapidly. In Fig. 3(b) is a plot of the effect of the Shirley background end-point smoothing number, m , for various thicknesses and for $I_{\text{Si}}^{\infty} = 800\,000$. This shows a significant improvement with m but note that the improvement in uncertainty for increasing m from 1 to 2 is already a factor of 1.24. Finally, in Fig. 3(c) we shown the strong improvement as I_{Si}^{∞} increases for various thicknesses but now for $m = 25$. In practice, we have found that $m = 25$ is a maximum useful value that leads to insignificant background distortion and maximum benefit in reducing U_n .

It is clear from Fig. 3 that the uncertainties increase rapidly above 6 nm and that thicknesses of >8 nm will have larger uncertainties arising from the fact that A_{Si} is $<5\%$ of A_{SiO_2} in this regime. It is also clear that, for 8 nm thickness, increasing m from 1 to 25 reduces the uncertainty from 0.066 to 0.037 nm. This smoothing, of course, takes no analytical time and significantly improves the result. Raising the counts by a factor of >3 would be needed to achieve the same result.

The uncertainty, U_n , gives the repeatability of the thickness measurement if we re-measure a sample without moving it. For repeat measures when the sample is moved, we must consider the instrument settings.

Geometry of the sample

The most sensitive part of the sample geometry is setting the angle of emission, θ . For (100) surfaces at the reference geometry this is at 34° to the surface normal, whereas for (111) surfaces the angle is reduced to 25.5° . There are two issues. An error in the value of θ causes a direct error in the value of $\cos\theta$ to be used in Eqns (2)–(5). An error of $+1^\circ$ at 34° directly leads to an error of $+1.2\%$ in d . A second error arises from the forward focusing and, although this has been minimized using the reference geometry, this will add linearly a further 0.4% to give a final 1.6% per degree of error. The precision of setting the angles, θ , is important. To evaluate a typical setting error in our instrument, which does not have a high-precision tilt stage, a laser system was devised to evaluate the repeatability of setting θ . This gave a standard deviation of 0.56° for tests done in a repeatability set, but over a longer term 0.75° is more reasonable. If we include this effect with that for the counting statistics, Figs 3(a) and 3(c) change as shown in Figs 4(a) and 4(b). For total counts over 400 000 in I_{Si}^{∞} , the uncertainty is dominated by the error in the angle setting and, approximately, at 34° for the (100) samples

$$U_\theta = 0.016 \quad \sigma_\theta d \quad (18)$$

where σ_θ is the standard uncertainty in setting the angular position (in degrees). For the 25.5° emission for (111) surfaces, the effect is as in Eqn. (18) with 0.016 reduced to 0.012.

RESULTS OF MEASUREMENTS AT NPL

To test the critical aspects of the uncertainties is not easy because we cannot easily record many sets of data. It takes

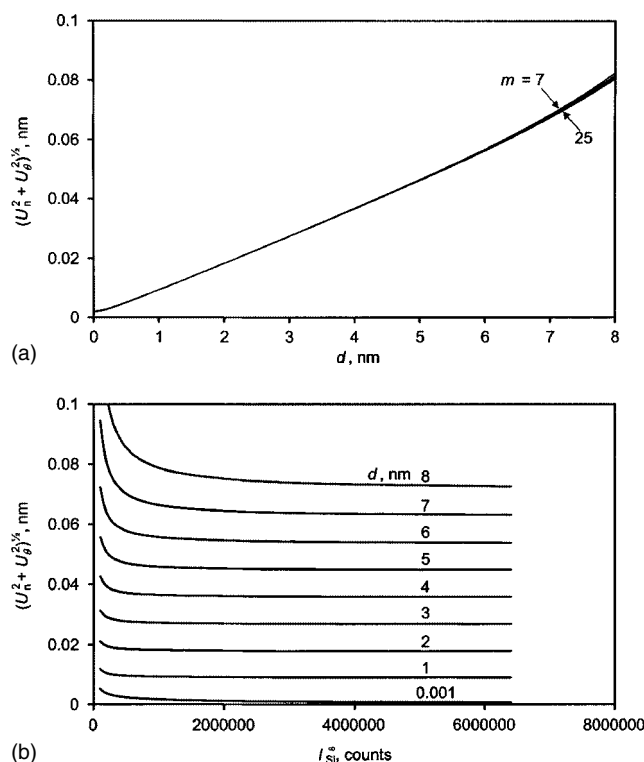


Figure 4. As Fig. 3 but with an added uncertainty from the angular setting of 0.56° : (a) as Fig. 3(a); (b) as Fig. 3(c).

1 day to record results for a full set of 10 samples. Using the reference geometry and the spectral details given earlier, we have twice measured two samples from our batches at the start of this work and again more recently after a period of 2 years. Briefly, the spectra are measured using a VG Escalab II spectrometer with five-channel electron multipliers using Mg x-rays and 20 eV pass energy with 6 mm input and output slits. The lens is set at a magnification of 3, with an input iris aperture restricting the angular acceptance to $\pm 6^\circ$ about the 34° and 25.5° angles of emission for (100) and (111) samples, respectively.¹² The geometry of the system is arranged so that the angle between the detected electron direction and the incident x-rays is 54.7° (the magic angle) so that the anisotropy terms may be ignored.

The above analysis gives a total of four measures for 10 samples of each of two sample sets, known as 'set 9' and 'set 12'. If we assume that the samples have not changed over the 2 years we can find the average thickness of each sample from the four measures and evaluate the deviation of each of the four results from the respective average for the two samples at each thickness. This will lead to a small overestimate of the uncertainties but, comprising eight results for each thickness, gives a useful measure. Figure 5(a) shows the standard deviation (SD, nm) as a function of thickness, d (nm), with the smaller uncertainties evident for the (111) samples. Figure 5(b) shows these data compared with the calculated uncertainty allowing for effects of the counting statistics with $I_{\text{Si}}^{\infty} = 800\,000$, $m = 25$ and the angular uncertainty of 0.56° added in quadrature. The correlation is excellent, bearing in mind the small number of results used to define the experimental standard deviations, and agrees with expectations from the relevant chi-squared distribution. For

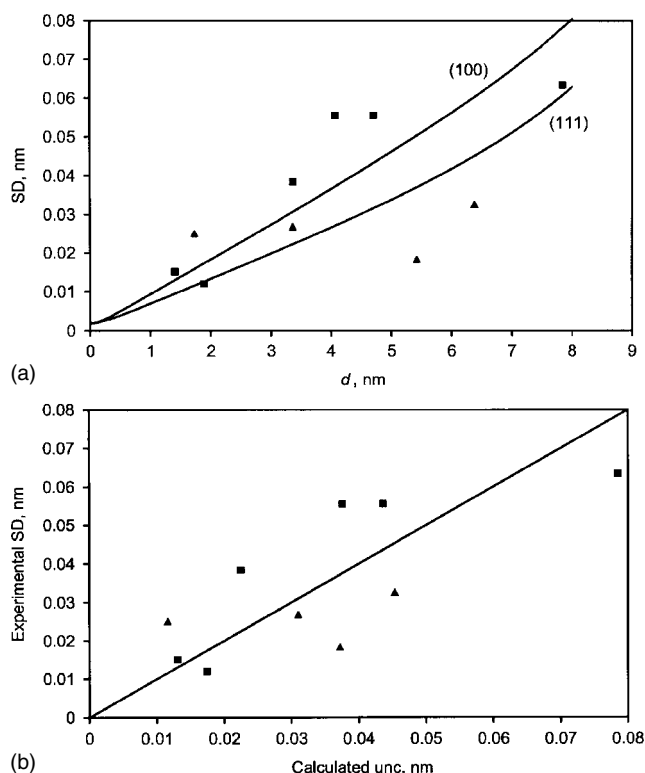


Figure 5. The average standard deviations (SD) of the four measurements each for sample sets 9 and 12 for each of the 10 thicknesses of (100) (■) and (111) (▲) surfaces versus: (a) the thickness with lines for the calculated uncertainty from the counting statistics with $I_{Si}^{\infty} = 800\,000$ and $m = 25$, with added uncertainty of 0.56° in the angular setting; (b) the calculated uncertainty where the line shows the line of perfect correlation.

a fit at a level of 10%, more than 100 measurements would be needed for each standard deviation. This correlation indicates that an angular repeatability uncertainty of 0.56° is consistent with these measurements.

Have the samples increased in thickness over the 2 years? Fig. 6 shows the increase in thickness averaged for the two sets of samples with the standard uncertainties

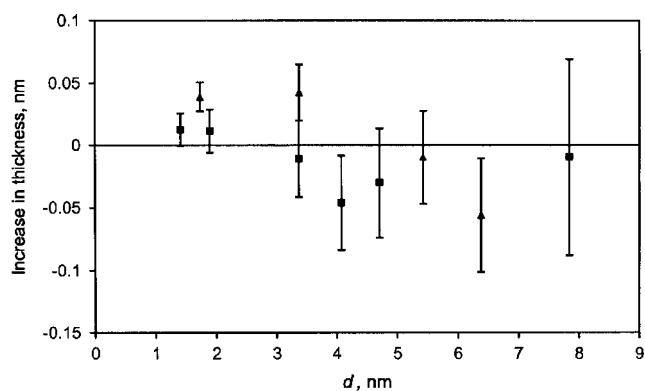


Figure 6. The increase in measured thickness, averaged for sets 9 and 12, for the 10 thicknesses over the interval of 2 years: ■ (100) and ▲ (111) surfaces. The standard uncertainties are calculated to include the statistical contribution with $I_{Si}^{\infty} = 800\,000$ and $m = 25$, with the angular contribution for $\sigma_{\theta} = 0.56^{\circ}$ added in quadrature.

added from the calculations with $I_{Si}^{\infty} = 800\,000$ counts, $m = 25$ and $\Delta\theta = 0.56^{\circ}$. Repeated measurements for the 4.7 nm (100) material, with sample removal, replacement and angular setting, gave a standard deviation of 0.029 nm .^{9,10} For the conditions of this work, the contribution from the statistics of the counting is 0.011 nm , and using the above σ_{θ} of 0.56° a total repeatability of 0.043 nm is predicted (as shown in Fig 6) that encompasses the measured value.

In Fig. 6, the value of no change in thickness is consistent with these data. They show the correct number of results covering zero as the uncertainty coverage factor is increased from zero to three. The overall increase in thickness is given by

$$\Delta d = -0.006 \pm 0.011\text{ nm} \quad (19)$$

where the uncertainty is the standard deviation of the mean. If we eliminate the two thickest samples with the greatest uncertainties, this changes to

$$\Delta d = 0.001 \pm 0.012\text{ nm} \quad (20)$$

Within these uncertainties, it is clear that the samples are stable. Furthermore, little advantage would be obtained in recording data for longer times or attempting more sophisticated analyses because the uncertainties are dominated by the 0.56° standard uncertainty in the repeatability of the angular setting. Note that there is a small advantage in using the (111) samples, where the uncertainty arising from the angular setting is reduced by a factor of 0.7 arising from the effects of emission closer to the surface normal.

So far we have not really considered the absolute uncertainties. The above uncertainties establish the repeatability in one laboratory.

UNCERTAINTY BETWEEN LABORATORIES

We can estimate the uncertainty of data between laboratories using the same analytical method (XPS) but different equipment and operators by using the data from the interlaboratory study conducted under the auspices of CCQM.^{9,10} These uncertainties will encompass contributions arising from the absolute angular settings and differences in the instrumental geometries, electron optics and software for data analysis. These laboratories did not study the same sample but samples from the same wafer. These wafers were not perfect and so were mapped by ellipsometry to ensure that the samples were characterized to 1% in thickness. We therefore expect the differences between an individual laboratory's data (laboratory 1) and the NPL data (laboratory 0) to be characterized by an uncertainty U_1 , where

$$U_1^2 = U_{1n}^2 + U_{1\theta}^2 + U_{1A}^2 + U_{1\beta}^2 + U_{1P}^2 + U_{1F}^2 + U_S^2 + U_0^2 \quad (21)$$

and U_{1n} , $U_{1\theta}$, U_{1A} and $U_{1\beta}$ are terms for the laboratory's statistics, emission angle setting, analyser electron optics and the effects of anisotropy. The terms U_{1P} and U_{1F} are terms for the use of different numbers of peaks in the fitting and the use of different algorithms by the laboratory, which we shall deal with later. Finally, there are uncertainties from

the sample to sample variation, U_s , and from the NPL data, U_0 , given by

$$U_0^2 = U_{0n}^2 + U_{0\theta}^2 + U_L^2 \quad (22)$$

where U_L is a type B uncertainty for the attenuation length. For comparative studies using XPS, U_L may be taken as zero because it biases all data equivalently. For absolute studies or comparison with other techniques, U_L needs inclusion. This is a small but non-zero term discussed at the end of this section.

In Fig. 7 we show the calculations for the (100) and (111) wafers for four typical conditions for I_{Si}^∞ and m , to show how the dependencies of U_1 on d , arising from the laboratories' contributions, are dominated by different terms in different regimes. In these plots we have taken U_s as 1%, because all samples were within 1% for thickness and $U_{1\theta}$ as 1°, in line with the general manufacturers' claims although, in individual cases, the angle setting could be biased up to 2°; with U_{1P} and U_{1F} at zero because valid software is not expected to lead to significant uncertainties. The terms described would lead to uncertainties of 1.9% and 1.5% for the (100) and (111) surfaces, respectively. The lowest curves in Fig. 7 for each surface for $I_{Si}^\infty = 800\,000$ and $m = 25$ approach these values and so, with typical commercial equipment and reasonable scan times using an unmonochromated x-ray source, the uncertainties are dominated by the quality of the test samples and the setting accuracy for the angle of emission of the detected electrons.

A further issue that needs consideration is the electron spectrometer. For accurate measurement of d , the solid angle of the spectrometer should be small. However, if monochromatic x-rays are used, to avoid low signals the designers have developed lenses of high solid angle. These can have acceptance angles up to $\pm 30^\circ$ from the lens axis, or even higher where magnetic lenses are involved. For angle-sensitive or angle-resolved data this angle should be reduced and in some cases was set to $\pm 4^\circ$ or $\pm 6^\circ$ but in others was $\pm 20^\circ$ or $\pm 30^\circ$. We may evaluate the effect of this larger aperture. We calculate, numerically, the intensities for

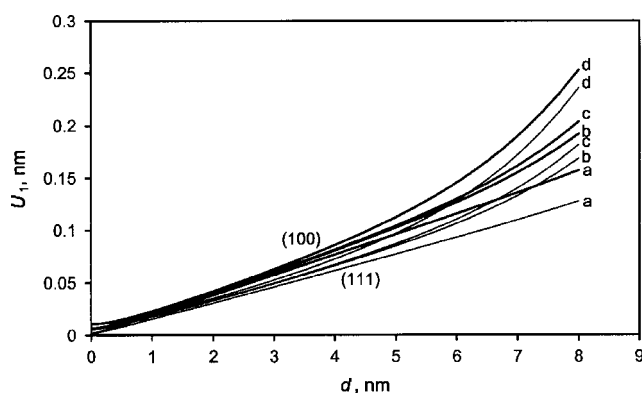


Figure 7. The uncertainty U_1 with $U_0 = 0$ as a function of the thickness for (100) and (111) surfaces for: (a) $m = 25$ and $I_{Si}^\infty = 800\,000$; (b) $m = 25$ and $I_{Si}^\infty = 80\,000$; (c) $m = 5$ and $I_{Si}^\infty = 80\,000$; (d) $m = 1$ and $I_{Si}^\infty = 80\,000$. The results for (100) and (111) surfaces are shown by thick and thin lines, respectively.

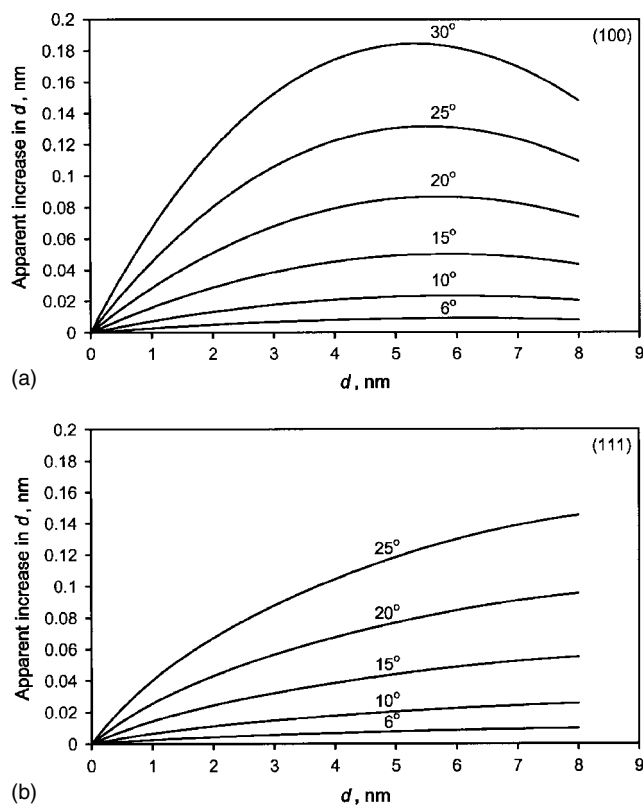


Figure 8. The bias, U_{1A} , or apparent increase in d as a function of the thickness for analyser entrance cone half-angles of up to 30° : (a) for the (100) surface; (b) for the (111) surface.

A_{SiO_2} and A_{Si} for Eqn. (17) for the 34° and 25.5° angles of emission for the (100) and (111) surfaces, respectively, as a function of the entrance solid angle and ignoring the effects of forward focusing. The error in the deduced thickness as a function of the thickness is shown in Fig. 8(a) for several entrance solid angles for the (100) geometry. The results for the (111) geometry are similar but rise more slowly, as shown in Fig. 8(b). For entrance solid angles up to $\pm 10^\circ$ the error is < 0.025 nm but this rises rapidly as the angle increases further. For comparison with experimental data, the results from Fig. 8 need to be combined with those from Fig. 7, but before we do this we should consider U_β , the effect of anisotropy.

There are few relevant direct calculations but the strength of the effect may be estimated from the data of Jablonski and Powell,²³ who have calculated the effects for the Si 2s peak in Si. For emission normal to the surface, they find that the attenuation length remains within a range of $\pm 2\%$ for $40^\circ \leq \gamma \leq 80^\circ$ and $1.5 \leq d \leq 5.5$ nm. The effect of changing γ is slow beyond 40° and also to higher thickness. By fitting their data for $45^\circ \leq \gamma \leq 90^\circ$ and $1.5 \leq d \leq 8$ nm, an effect of $\pm 1.9\%$ encompasses the full range. The β value for the anisotropy of the Si 2p peak is approximately half the value for the 2s peak²⁴ and so we may expect the above effect to be halved. Furthermore, the overlayer of SiO_2 has a lower value of the single scattering albedo, ω , than for Si, so the whole range of the effect for $45^\circ \leq \gamma \leq 90^\circ$ and $1.5 \leq d \leq 8$ nm will be encompassed by $\pm 0.75\%$ or a standard uncertainty of 0.4%. Added in quadrature, this small contribution may be

ignored here but should always be included, formally, in case accuracies improve. We should now look at the experimental results from the interlaboratory study.^{9,10}

In this study there were nine sets of data, as shown in Table 1, but in one of these data sets the background subtraction method was not a Shirley background but either a straight-line or oversmoothed function, the latter leading to significant reduction in the oxide peak area measured. The remaining eight data sets will be analysed here. In the report of the wider interlaboratory study, responsee results were compared with the NPL data according to Eqn. (1) to evaluate the scaling term, $m_{\text{responsee}}$, the offset, $c_{\text{responsee}}$, and the rms scatter of the data about the best-fit line, $r_{\text{responsee}}$. For all eight laboratories listed, the averages and standard deviations are $m_{\text{responsee}} = 0.998 \pm 0.028$, $c_{\text{responsee}} = -0.021 \pm 0.121$ and $r_{\text{responsee}} = 0.077$. This shows that the overall results were excellent and far better than had been expected at the outset, where many analysts were anticipating uncertainties of 20% associated mainly with L_{SiO_2} . However, for considering uncertainties Eqn. (1) is not quite what we need here. We consider the absolute differences, Δ , where

$$\Delta = d_{\text{responsee}} - d_{\text{NPL}} \quad (23)$$

This is shown in Fig. 9 for the seven laboratories. If we evaluate the means and the standard deviations for each thickness, we obtain the results of Fig. 9(b). The standard deviations of the means (not shown) all bracket the zero line, showing that there is no inconsistency in this set of data and the NPL data. The rms values for the scatters, shown in Fig. 9(c), average 0.17 nm. Also shown on Fig. 9(c) is the quadrature calculation, including U_0 , for the results of a 20° lens entrance half-angle and U_1 , assuming $\sigma_\theta = 1^\circ$, $U_S = 1\%$ and $U_{1P} = 0.6\%$. The value of U_{1P} is taken from the calculations given elsewhere¹⁵ relevant to Eqn. (2). The curves for the (100) and (111) samples differ slightly, arising from the lower angle of emission used in the (111) samples.

Very broadly, the main contributions to the result for the (100) surfaces in Fig. 9(c) arise from 1.6% for the 1° angular accuracy ($U_{1\theta}$), 1% for the sample-to-sample variation (U_S), 1.4% for the entrance solid angle of the analyser (U_{1A}), 0.6% for the use of different numbers of peaks (U_{1P}) and 1% for the NPL data (U_0). These amount, in quadrature, to most of the 2.6% shown. It is not clear why some of the results for the (100) surfaces below 5 nm are biased to higher scatters than expected, but broadly the results are consistent with the levels of accuracy expected.

Clearly, if analysts could use a more accurate setting for the angle of emission, smaller entrance solid angles to their analysers and consistent analytical procedures, the three largest uncertainty terms could be reduced. However, at the present time we do not know how much better the final laboratory-to-laboratory scatter would be. In the spirit of assessing 95% confidence limits using an expansion factor of 2, the experimental results of Fig. 9(c) currently indicate that laboratories generally can achieve an uncertainty of 0.4 nm over the range $2.5 < d < 7.8$ nm, with a lower value of 0.25 nm for $d < 2.5$ nm.

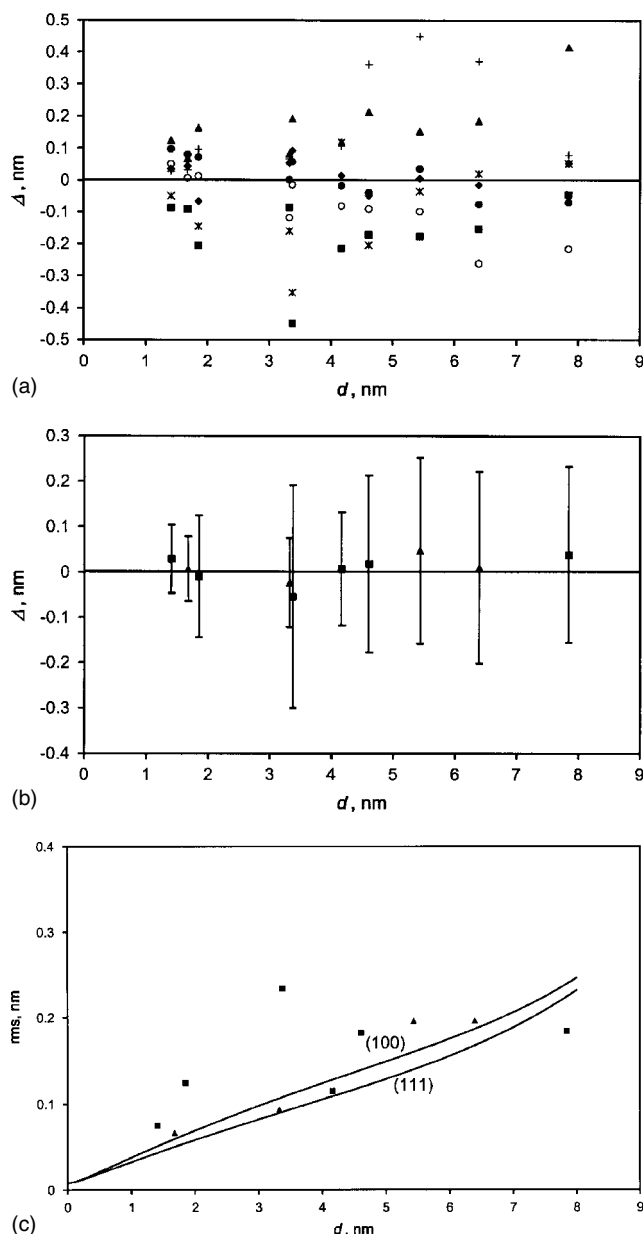


Figure 9. Scatters from seven laboratories using the reference geometry in the interlaboratory study,^{9,10} calculated from the absolute difference, Δ , from the NPL data as a function of the oxide thickness. (a) Individual results for Δ : (◆) BAM, (▲) University of Utsunomiya, (+) NUS, (■) CSIR, (★) EMPA, (○) Philips 1 and (●) Philips 2. (b) Means and standard deviations for (100) (■) and (111) (▲) samples. (c) The rms values from the distributions about zero, and the calculated uncertainties for (100) and (111) surfaces.

There is one final uncertainty that we have not addressed: the value of the attenuation length, L_{SiO_2} . In the interlaboratory study^{9,10} it was found that L_{SiO_2} should be scaled from the values of 2.964 and 3.448 nm for Mg and Al x-rays,¹² respectively, by the factor 0.986 ± 0.009 at 95% confidence. Thus, all of the thicknesses cited here should be reduced by 1.4% and a further uncertainty, U_L , of 0.45% should be added. This does not affect the above analyses but does need to be included for a final expression of the measurement uncertainty. This increases the 0.4 nm uncertainty figure for

the results from the interlaboratory study to 0.41 nm for the seven thicker oxides and does not represent a major issue. The attenuation length contribution is more significant in the relatively more accurate NPL data. For these measurements, for comparison between XPS results, we may approximate the calculated results of the direct NPL data of Fig. 5 to be

$$U_0 \leq 0.010d \quad \text{for (100) surfaces} \quad (24)$$

$$U_0 \leq 0.008d \quad \text{for (111) surfaces} \quad (25)$$

For absolute comparisons or comparisons between techniques, however, U_L needs inclusion and we finally obtain

$$U_0 \leq 0.011d \quad \text{for (100) surfaces} \quad (26)$$

$$U_0 \leq 0.009d \quad \text{for (111) surfaces} \quad (27)$$

CONCLUSIONS

Analysis shows that improvements to precisions in measuring the layer thicknesses may be made by ensuring that data are acquired with adequate statistics and that the peak synthesis is conducted with valid software using relevant algorithms. Further improvements may be made by ensuring that the end-points for the background have adequate averaging, unless the software is designed to fit the background with the peaks. For total peak areas, I_{Si}^∞ , of $>800\,000$ counts, the contribution from counting statistics is $<0.5\%$ and may be dominated by other terms.

For spectrometers with entrance cone angles that may be limited to less than $\pm 10^\circ$ the setting of the emission angle becomes an important term, otherwise the entrance solid angle can be the dominant term. Using the NPL spectrometer, 0.56° repeatability in θ has been measured, leading to a standard uncertainty of 0.9% in (100) data and 0.6% in (111) data measured at reference geometry settings of 34° and 25.5° angles of emission, respectively. Typical values for the repeatability and accuracy in θ in commercial instruments could be 1° , leading to standard uncertainties of 1.6% and 1.2% for the (100) and (111) surfaces, respectively.

For spectrometers with larger solid angles, increases in thickness of up to 5% may be found. In a comparison of results from seven laboratories, a further 1% standard uncertainty is expected to arise from the consistency of the test samples. Some additional further uncertainty arises from the use of different software algorithms and the use of different procedures and numbers of peaks in the analysis, and leads to results with a final uncertainty at 95% confidence of 0.4 nm over the range $2.5 < d < 7.8$ nm, with a lower value of 0.25 nm for $d < 2.5$ nm.

Added to the above uncertainties is the uncertainty in the relevant attenuation length for use with these equations, and here a standard uncertainty of 0.45% must be incorporated.

This causes an insignificant increase to the 0.4 nm of the interlaboratory study but does affect the NPL data, as shown in Eqns (26) and (27). Thus, with care, it is shown that the standard uncertainties can be reduced to 1%.

Acknowledgements

The author would like to thank the interlaboratory respondents for their contributions, S.J. Spencer for the original NPL data and for arranging the figures for publication and I.S. Gilmore for comments. This work is supported by the National Measurement System of the UK Department of Trade and Industry through the Valid Analytical Measurements Programme.

REFERENCES

1. Briggs D, Seah MP. *Practical Surface Analysis, Vol 1: Auger and X-ray Photoelectron Spectroscopy*. Wiley: Chichester, 1990.
2. Briggs D, Seah MP. *Practical Surface Analysis, Vol 2: Ion and Neutral Spectroscopies*. Wiley: Chichester, 1992.
3. ISO 24237 (in draft). *Surface Chemical Analysis—Auger electron spectrometers—Repeatability of intensity scale*. ISO: Geneva, 2004.
4. ISO 24236 (in draft). *Surface Chemical Analysis—X-ray photoelectron spectrometers—Repeatability of intensity scale*. ISO: Geneva, 2004.
5. Gilmore IS, Seah MP. In *Secondary Ion Mass Spectrometry, SIMS XI*, Gillen G, Lareau R, Bennett J, Stevie F (eds). Wiley: Chichester, 1998; 999.
6. Gilmore IS, Seah MP. *Surf. Interface Anal.* 2000; **29**: 624.
7. Seah MP, Gilmore IS, Spencer SJ. *J. Electron Spectrosc.* 1999; **104**: 73.
8. ISO 21270. *Surface Chemical Analysis—X-ray photoelectron and Auger electron spectrometers—Linearity of intensity scale*. ISO: Geneva, 2004.
9. Seah MP. *J. Vac. Sci. Technol. A* 2004; **22**: 1564.
10. Seah MP, Spencer SJ, Bensebaa F, Vickridge I, Danzebrink H, Krumrey M, Gross T, Oesterle W, Wendler E, Rheinländer B, Azuma Y, Kojima I, Suzuki N, Suzuki M, Tanuma S, Moon DW, Lee HJ, Cho HM, Chen HY, Wee ATS, Osipowicz T, Pan JS, Jordaan WA, Hauert R, Klotz U, van der Marel C, Verheijen M, Tamminga Y, Jeynes C, Bailey P, Biswas S, Falke U, Nguyen NV, Chandler-Horowitz D, Ehrstein JR, Muller D, Dura JA. *Surf. Interface Anal.* 2004; **36**: 1269.
11. Seah MP, Spencer SJ. *J. Vac. Sci. Technol. A* 2003; **21**: 345.
12. Seah MP, Spencer SJ. *Surf. Interface Anal.* 2002; **33**: 640.
13. Seah MP, White R. *Surf. Interface Anal.* 2002; **33**: 960.
14. Cole DA, Shallenberger JR, Novak SW, Moore RL, Edgell MJ, Smith SP, Hitzman CJ, Kirchhoff JF, Principe E, Nieveen W, Huang FK, Biswas S, Bleiler RJ, Jones K. *J. Vac. Sci. Technol. B* 2000; **18**: 440.
15. Seah MP, Spencer SJ. *Surf. Interface Anal.* 2003; **35**: 515.
16. Hollinger G, Himsel FJ. *Appl. Phys. Lett.* 1984; **44**: 93.
17. Keister JW, Rowe JE, Kolodziej JJ, Niimi H, Tao H-S, Madey TE, Lucovsky GJ. *J. Vac. Sci. Technol. A* 1999; **17**: 1250.
18. Shirley DA. *Phys. Rev. B* 1972; **5**: 4709.
19. *Guide to the Expression of Uncertainty in Measurement*. ISO: Geneva, 1993.
20. Seah MP, Tosa M. *Surf. Interface Anal.* 1992; **18**: 240.
21. Seah MP. *Surf. Interface Anal.* 1995; **23**: 729.
22. Seah MP, Brown MT. *J. Electron Spectrosc.* 1998; **95**: 71.
23. Jablonski A, Powell CJ. *Surf. Sci. Rep.* 2002; **47**: 33.
24. Yeh JJ, Lindau I. *At. Data Nucl. Data Tables* 1985; **32**: 1.